EUROPHYSICS LETTERS 15 April 2005

Europhys. Lett., **70** (2), pp. 264–270 (2005)
DOI: 10.1209/epl/i2004-10478-8

Dynamic surface decoupling in a sheared polymer melt

X. Zhou, D. Andrienko, L. Delle Site and K. Kremer
Max-Planck-Institut für Polymerforschung - Ackermannweg 10, 55128 Mainz, Germany

received 21 December 2004; accepted in final form 18 February 2005
published online 11 March 2005

PACS. 83.80.Sg – Polymer melts.
PACS. 61.20.Ja – Computer simulation of liquid structure.
PACS. 47.27.Lx – Wall-bounded thin shear flows.

Abstract. – We propose that several mechanisms contribute to friction in a polymer melt adsorbed at a structured surface. The first one is the well-known disentanglement of bulk polymer chains from the surface layer. However, if the surface is ideal at the atomic scale, the adsorbed parts of polymer chains can move along the equipotential lines of the surface potential. This gives rise to a strong slippage of the melt. For high shear rates chains partially desorb. However, the friction force on adsorbed chains increases, resulting in quasi-stick boundary conditions. We propose that the adsorbed layers can be efficiently used to adjust the friction force between the polymer melt and the surface.

Introduction. – Frictional forces between solid substrates can be dramatically reduced by coating them with thin polymer layers, which are able to sustain large normal loads while remaining fluid [1]. This effect has obvious practical applications, ranging from biolubrication to hard-disk drives [2]. The molecular mechanism of friction, however, is still poorly understood [3]. It is believed that the striking reduction of shear forces in systems with end-adsorbed and grafted polymers immersed in liquids is due to limited mutual interpenetration of the brushes in good solvent, even under compression, and a fluid interfacial layer where most of the shear occurs. In polymer melts the situation is very different, because of the dominance of entanglement effects (if the chains are long enough), associated high viscosities, and screening of the excluded-volume interactions [4, 5]. In spite of these differences, the key parameter affecting the lubrication and shear forces is still the degree of interdigitation between the moving surface layer and the bulk polymer system [6]. Regarding the structure of the adsorbed polymer layers, two systems were thoroughly examined, both theoretically and experimentally: i) Polymer brushes with the chains tethered by one end to a solid surface. At high enough coverage, the chains stretch away from the surface and form a brush-like structure. ii) Melt layers which are formed when a strongly attractive surface is exposed to a polymer melt and a certain amount of polymer becomes permanently bound to the surface. The resulting layer is made of loops, with a large polydispersity of loop sizes, reflecting the statistics of the chains in the melt [7, 8]. As to the rheological properties of brushes, it is now well accepted that the polymer anchoring on solid surfaces plays a key role on the flow behavior of polymer melts, in particular on the appearance of flow with *slip* at the wall [9, 10]. The onset of wall slip is related to the strength of the interactions between the solid surface and

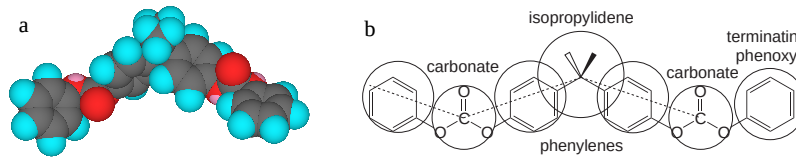

Fig. 1 – (a) Chemical structure and (b) coarse-graining scheme of bisphenol-*A* polycarbonate. Corresponding comonomeric groups (isopropylidene, carbonate, and two phenylenes) are replaced by four beads. Only the chain end and one repeat unit are shown.

the melt: if there is a finite slip velocity v_s at the interface, the shear stress at the solid surface can be evaluated as $\tau_{xz} = \beta v_s$, where β is the friction coefficient between the fluid molecules in contact with the surface and the solid surface. On the other hand, $\tau_{xz} = \eta(\mathrm{d}v/\mathrm{d}z)_{z=0}$, where η is the melt viscosity. Introducing the extrapolation length (slip length) b of the velocity profile to zero ($b = v_s/(\mathrm{d}v/\mathrm{d}z)_{z=0}$), one obtains $\beta = \eta/b$. Thus, determination of b will yield β, the friction coefficient between the surface and the fluid, which is directly related to the molecular interactions between the fluid and the solid surface [6].

The appearance of wall slip in polymer melts can be expected from the analogous phenomenon in simple liquids [11, 12], which still poses unresolved challenges in understanding [13]. Typical model systems assume that chain ends (or parts of the chain) are fixed at the surface [8, 9, 14]. However, reasonably weak coupling might result in partial or complete detachment of the chains. This certainly will be the case for most adsorbing chain ends or fragments (*i.e.* for block copolymers). In addition, the attached parts of the chains can travel along the equipotential lines of the surface or along minimal activation paths. In this work we thus focus on the situation where the surface bonding is strong but reversible. As an example, we consider a bisphenol-A polycarbonate (BPA-PC) melt sheared over a (111) nickel surface. The inner parts of the polymer chains are repelled from the surface and only one of the comonomeric groups (phenol) is attracted to it. Internal phenylenes are, however, sterically hindered to adsorb by the rest of the groups. On the contrary, chain ends can easily adsorb to the surface; a large adsorption energy (about $20kT$ at the processing temperature of 570 K) prevents the adsorbed chains from a spontaneous desorption. A closer look at the structure and packing of short but experimentally relevant polymer chains at the walls shows that there are two distinct (overlapping) layers, formed by the single- and two-end adsorbed chains. The layer composed of the two-end adsorbed chains is made of highly entangled loops, with the configurations reflecting the statistics of the chains in the melt. The single-end adsorbed chains are stretched and form a brush-like layer, which is strongly interdigitated with the bulk of the melt [15–18]. The complex structure of the surface layer enriches the behavior of the sheared melt: in addition to large slip length and decoupling of the surface layer from the bulk, we also observe the transient regime, when the two-end attached chains are practically unaffected by shear, but the single-end attached chains are stretched and form a (lubricating) layer between the two-end adsorbed and bulk chains. For even higher shear rates we observe shear-induced desorption of the single-end adsorbed chains, which affects both the width of the adsorbed layer and the value of the slip length.

Model and interaction potentials. – The coarse-grained model is discussed in previous works [15, 17]. Briefly, each repeat unit (carbonate, isopropylidene, and two phenylenes) of a BPA-PC chain is replaced by four different beads, as shown in fig. 1. All beads interact with each other via shifted repulsive Lennard-Jones potential. The sizes of the beads are such that the volume of the repeat unit, accounting for overlaps, is equal to the van der Waals volume per

repeat unit computed from the equation-of-state analysis [19]. Intramolecular bond-angle and harmonic spring potentials reflect the Boltzmann distribution of the corresponding variables for a single chain in vacuum.

The bead-wall interaction potential reflects the structure of the surface. Expanding this potential in two-dimensional reciprocal lattice space and performing the summation over the reciprocal vectors of the same length we obtain

$$U(x,y,z) = \sum_i U_i(z)\, f_i(x,y), \tag{1}$$

where $i = 0, 1, 2, \ldots$ corresponds to the reciprocal vectors of different lengths, $f_i(x,y)$ are linear combinations of trigonometric functions. Expansion (1) can be used for a surface of any symmetry. To proceed further, we make use of the fact that the (111) surface of the nickel fcc lattice has the C_6 symmetry. Restricting ourselves to the first three terms in (1), we obtain $f_0 = 1$, $f_1 = \cos(\bar{x} - \bar{y}) + \cos(\bar{x} + \bar{y}) + \cos 2\bar{y}$, and $f_2 = \cos(\bar{x} - 3\bar{y}) + \cos(\bar{x} + 3\bar{y}) + \cos 2\bar{x}$, where $(\bar{x}, \bar{y}) = \frac{2\pi}{a}\,(x, \frac{y}{\sqrt{3}})$. The z-dependent prefactors $U_i(z)$ are obtained from the *ab initio* calculations [20]. These calculations show that the adsorption energies of both carbonate and isopropylidene are rather small, much smaller than the characteristic thermal energy in a melt at processing temperature; below 3.2 Å, they experience strong repulsion from the nickel surface. Contrary, the phenolic group is attracted by the surface, with adsorption energy about 1 eV at an optimal distance $z_0 = 2$ Å; the adsorption is short-ranged and decays below 0.03 eV at a distance beyond $z_c = 3$ Å. Because of that the internal phenylenes are sterically hindered by the neighboring comonomeric groups to adsorb. We assume that they interact with the walls via a 10-4 repulsive potential. The chain ends are not hindered by their nearest neighbors. The results of the *ab initio* calculations suggest a simple piecewise function for the attractive surface-phenoxy bead interaction potential at a bridge site [17]

$$U_0 = \begin{cases} \frac{5}{3}\epsilon_r \left[\frac{2}{5}\left(\frac{z_0}{z}\right)^{10} - \left(\frac{z_0}{z}\right)^4 + \frac{3}{5}\right] - \epsilon_0\,, & z < z_0\,, \\ \frac{\epsilon_0}{2}\left[\cos\left(\pi\frac{z_c - z}{z_c - z_0}\right) - 1\right], & z_0 \le z < z_c\,. \end{cases}$$

Ab initio results also suggest that the *functional form* of the z-dependent part of the potential is practically independent of the xy position of the bead, only the well depth (ϵ_0) of the potential changes. At an optimal distance $z = 2$ Å the adsorption energies are: $U_{\text{atop}} = -0.1$ eV, $U_{\text{bridge}} = -0.9$ eV, $U_{\text{hollow}} = -0.8$ eV [20]. Adopting these values and assuming the same functional form for the attractive part of $U_{0,1,2}(z)$, we obtain

$$U_{1,2} = \begin{cases} -\epsilon_{1,2}\,, & z < z_0\,, \\ \frac{\epsilon_{1,2}}{2}\left[\cos\left(\pi\frac{z_c - z}{z_c - z_0}\right) - 1\right], & z_0 \le z < z_c\,, \end{cases} \tag{2}$$

where an excellent agreement is obtained for $\epsilon_r = 1.5$ eV, $\epsilon_0 = 0.7$ eV, $\epsilon_1 = -7/45$ eV, and $\epsilon_2 = -2/45$ eV. The $U_i(z)$ prefactors, as well as the final potential and the *ab initio* data, are shown in fig. 2(a). The contour plot of the surface potential is depicted in fig. 2(b).

Simulation details. – BPA-PC melt is confined to a slit pore comprised of two parallel (111) nickel surfaces. The pore width is set to $L_z = 48.54\sigma$. The normal to the surfaces is parallel to the z-axis. The sample consists of 240 BPA-PC molecules of $N = 20$ repeat units. Because of the small entanglement length of BPA-PC ($N_e = 6$), these chains are already weakly entangled. The units are chosen such that $kT = 1$ with $T = 570\,K$, *i.e.* 1 eV

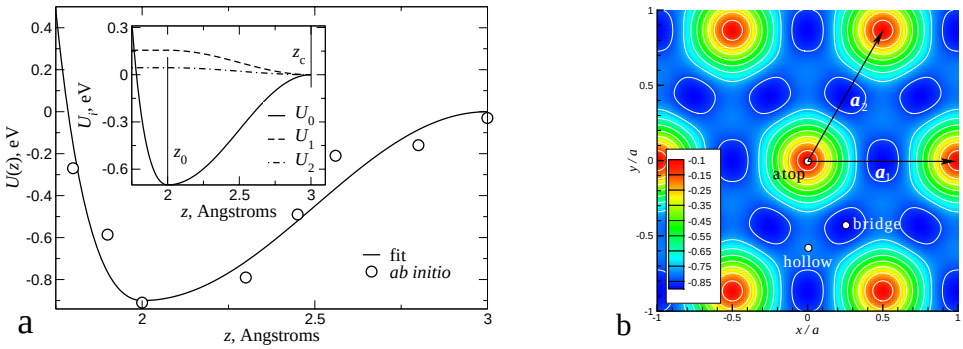

Fig. 2 – (a) Wall-phenoxy bead interaction potential taken at a bridge site. Open circles: results of *ab initio* calculations. Solid line: fit to eq. (1). The inset shows the prefactors $U_{0,1,2}(z)$. (b) Contour plot of the attractive potential between the terminating phenoxy and the wall at a distance $z_0 = 2$ Å. Three values matched the *ab initio* data: $U_{\text{atop}} = -0.1$ eV, $U_{\text{bridge}} = -0.9$ eV, $U_{\text{hollow}} = -0.8$ eV.

corresponds to about $20\,kT$; the unit of length is $\sigma = 4.41$ Å. Periodic boundary conditions are employed in x and y directions. The x and y box dimensions are set to $L_x = 22.23\,\sigma$ and $L_y = 21.72\,\sigma$, which corresponds to a (111) hexagonal lattice of nickel with 39 and 22 unit cells (the unit lattice constant of the hexagonal lattice is about $a = 0.57\,\sigma$). The system density is fixed at $0.85\sigma^{-3}$, which corresponds to 1.05 g/cc, the experimental density at $T = 570$ K. Starting configurations are generated by randomly placing the chains in the simulation box. A short run is then used to remove the bead-bead overlaps [17]. Then the system is equilibrated during 10^8 timesteps. The production run is performed in the NVT ensemble with Langevin thermostat with friction $0.5\tau^{-1}$. The thermostat is switched off in the shear direction (along the x-axis). The velocity-Verlet algorithm with the timestep $\Delta t = 0.005\tau$ is used to integrate the equations of motion. The top and bottom walls move (in opposite directions) at constant velocity v_w, so that the shear rate is $\dot\gamma = 2v_w/L_z$. We use $v_w\tau/\sigma = 0$, 0.001, 0.01, and 0.1 or $s = \dot\gamma\tau_r \approx 0$, 2, 20, and 200, respectively, where $\tau_r \approx 5 \times 10^4\tau$ is the characteristic relaxation time of a single chain of BPA-PC in bulk [21]. Note that we apply rather high shear rates, of the order of $10^5\,\text{s}^{-1}$. However, the average chain length in a BPA-PC melt is $N \approx 70$ and, therefore, the corresponding chain reptation time $\tau_d \sim N^{3.4}$ is almost by two orders of magnitude bigger than that of the $N = 20$ chains. Equivalently, shear rates would be reduced by almost two orders of magnitude, close to the values used to process the melt.

Results. – The snapshots of the systems, for different shear rates, are shown in fig. 3. The increase of the shear rate results in chain stretching. For small shear rates, fig. 3(b), the change in the chain configurations is practically negligible compared to the system without shear, fig. 3(a). For medium shear rates, fig. 3(c), the chain conformations, as well as the width of the layer formed by the two-end adsorbed chains, does not change. The chains adsorbed with one end stretch and form a thin layer between the bulk and the chains adsorbed with two ends. The chains in the bulk decouple from this layer. Finally, for even higher shears, fig. 3(d), the single-end attached chains stretch even more; almost all of them desorb and move into the bulk. As a result, the layer made of adsorbed chains shrinks.

Keeping this qualitative picture in mind, let us quantify our results. We first have a look at the changes in the bead density profiles, shown in fig. 4. For medium shear rates ($v_w = 0.01\,\sigma/\tau$, $\dot\gamma\tau_r = 20$) the layering of the beads next to the wall extends to a depth of about the radius of gyration $R_g \sim 7\sigma$, similar to the system without shear. The chain end

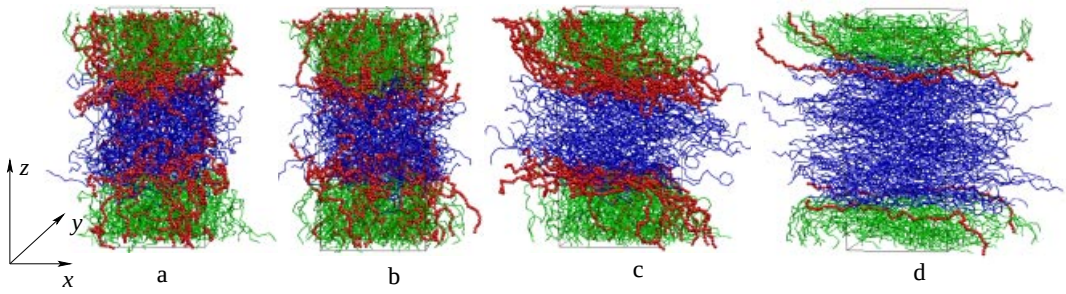

Fig. 3 – Snapshots of the system for different wall velocities: (a) no shear; (b) $v_w = 0.001\sigma/\tau$; (c) $v_w = 0.01\sigma/\tau$; (d) $v_w = 0.1\sigma/\tau$. Polymer chains are divided into three populations: chains which adsorb both ends (green), only one end (red), and no ends on the surface (blue).

density has a large peak next to the wall; then the region with practically no ends (depleted region) follows; finally, the bulk concentration of the ends is reached at a distance of about $2R_g$. If we increase the shear rate, the density of the ends at the wall decreases, as shown in the left inset of fig. 4. At the same time, the depleted layer shrinks, as illustrated in the right inset of the same figure. Both effects are due to desorption of the chain ends from the walls, as well as stretching and tilting of the chains under shear.

More information about the chain conformations at the surface and in the bulk can be obtained from the center-of-mass density profiles, shown in fig. 5. The chains are divided into two categories: those chains with two ends adsorbed and those chains with only one end adsorbed on the wall. Without shear, the profiles are similar to those reported before [17]: any chain with the center of mass in the layer next to the wall has both ends adsorbed on the surface. The next layer contains a majority of chains with a single end adsorbed. The single-end adsorbed chains mix well with the bulk of the melt. For small shear rates ($\dot{\gamma}\tau_r = 2$) the changes in the layers are not detectable. However, for higher shear rates, several different scenarios develop. For $\dot{\gamma}\tau_r = 20$, the layer of single-end adsorbed chains becomes narrower; the center-of-mass density drops down almost to zero immediately after it, *i.e.* a layer of

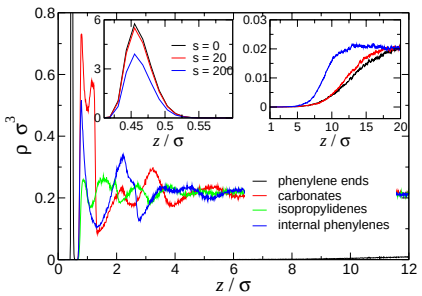

Fig. 4

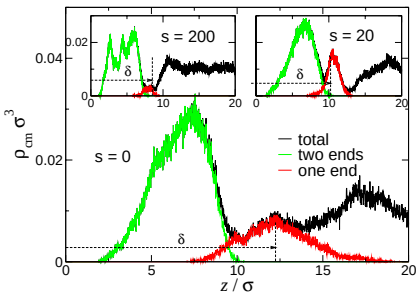

Fig. 5

Fig. 4 – Number density profiles of beads in a sheared melt for $s = \dot{\gamma}\tau_r = 20$. Insets: zooms in the chain-end density profiles at small and large distances from the wall, for different shear rates.

Fig. 5 – Center-of-mass density profiles, showing division into populations of chains which adsorb both ends to the surface (green), one end on the surface (red), and the total center-of-mass density (black). Insets illustrate changes in the profiles for different shear rates.

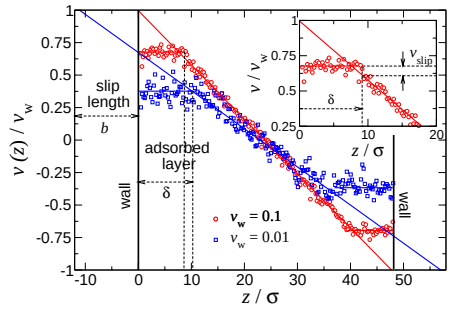

Fig. 6 – The normalized velocity profiles for two shear rates. Symbols: simulation results. Solid lines: fit to a constant or a linear function, depending on the layer.

single-end adsorbed chains is formed on the top of the layer of double-end adsorbed chains; the bulk chains detach from these two layers. Again, the layer of the adsorbed (both with one and two ends) chains shrinks compared to the static case, due to stretching and alignment of adsorbed chains. If we increase the shear rate ($\dot{\gamma}\tau_r = 200$), the single-end adsorbed chains desorb and additional layers due to the chain dense packing at the wall appear.

Finally, fig. 6 shows the velocity profiles normalized to the wall velocity. For all shear rates, the profiles have similar features: i) next to the wall it is practically constant, *i.e.* the adsorbed chains are dragged by the wall. The flat plateau has the same width as the adsorbed layer, measured from the center-of-mass density profiles, fig. 5. Immediately after the plateau the velocity profile becomes a linear function of z. The transition region is very small, again due to the fact that the adsorbed and bulk polymer chains are very much decoupled. ii) the velocity of the beads at the walls (v_s) is smaller than the wall velocity, *i.e.* even though the chain ends strongly adsorb on the wall they can still slide over it. This is not surprising —an adsorbed bead can hop between the hollow to bridge sites, since the difference in the adsorption energies of these two sites is small, of the order of 0.1 eV.

Let us denote the thickness of the adsorbed layer as δ and the velocity of this layer as v_s. Then the bulk velocity can be written as $v = v_s(L-2z)/(L-2\delta)$. The slip length b, obtained from the condition $v(z = -L/2 - b) = v_w$, reads

$$b = (v_w/v_s - 1)\, L/2 - \delta v_w/v_s\,. \tag{3}$$

It can be seen that two mechanisms contribute to the total slip length b. The first one is due to the apparent slip of the adsorbed layer over the surface. The second, negative, contribution is due to the finite thickness of the adsorbed polymer layer. Examining the velocity profiles we see that for $s = 20$ the apparent slip dominates and results in a slip length of the order of 10σ. For higher shear rates, $s = 200$, the two contributions compensate each other, even though δ decreases, again due to the fact that v_s/v_w increases with the increase of the shear rate. Another possible contribution to the total slip length is shown in the inset of fig. 6. Here the bulk of the melt slips over the wall-adsorbed layer. This contribution is, however, rather small. Finally, for the friction coefficient $\beta = f_x/(v_w - v_s)$, where f_x is the friction force per unit areal, we obtain $\beta(s = 20) = 4.4$ and $\beta(s = 200) = 3.9$ (β is given in units of $kT\,\tau\,\sigma^{-4}$). Therefore, in spite of the fact that the higher shear rates lead to a reduction of slip length, the surface friction itself decreases. In fact, it is the disentanglement of the bulk polymer chains from the surface layer which is responsible for this decrease.

To conclude, we have studied a shear of a BPA-PC melt over a (111) nickel surface as a specific test case of a more general phenomenon of shear of an adsorbing polymer melt over

structured surfaces. We find that two mechanisms contribute to the kinetic friction and effective hydrodynamic boundary conditions. The first mechanism is similar to the one observed when an adsorbed surface layer (either solid or liquid) slides over a structured substrate [22]. The substrate potential induces the density modulation in this layer, and energy is lost from these modulations through the anharmonic coupling to the thermostat. In our case, the attached chain ends move along surface minimal activation paths and the energy loss is due to their scattering on the wall potential and coupling of the rest of the chain to the thermostat. On the other hand, we also observe that the one-end-attached chains undergo a coil/stretch transition and disentangle from the melt, in agreement with the theoretical predictions for grafted chains [9, 10]. In principle, stretching should lead to large slip lengths at high shear rates. For our system, however, the net effect of chain stretching is much smaller than the energy dissipation in the adsorbed layer. All together, competition between these two mechanisms, combined with the ability of chains to desorb, results in a nontrivial friction law, with both the slip length and the friction force depending on the shear rate.

Possible implication of our work is that the surface-anchored layers can be efficiently used to adjust the friction between polymer melt and a surface. This can be done by changing the surface concentration of one- and two-end adsorbed chains by, for example, additives occupying the attractive sites of the nickel surface [23].

* * *

This work was supported by the Alexander von Humboldt Foundation, Germany (XZ) and by the BMBF, under Grant No. 03N6015. Advise of B. DÜNWEG is acknowledged.

REFERENCES

[1] KLEIN J., *Annu. Rev. Mater. Sci.*, **26** (1996) 581.
[2] JIN Z. M. *et al.*, *Wear*, **170** (1993) 281; MA X., *IEEE Trans. Magn.*, **35** (1999) 2454.
[3] GREST G. S., *Adv. Polym. Sci.*, **138** (1999) 149; PERSSON B. N. J., *Surf. Sci. Rep.*, **33** (1999) 85; RINGLEIN J. and ROBBINS M. O., *Am. J. Phys.*, **72** (2004) 884.
[4] YAMAMOTO R. and ONUKI A., *Phys. Rev. E*, **70** (2004) 041801.
[5] EVERAERS R. *et al.*, *Science*, **303** (2004) 823.
[6] LÉGER L., RAPHAËL E. and HERVET H., *Adv. Polym. Sci.*, **138** (1999) 185.
[7] AUBOUY M., GUISELIN O. and RAPHAEL E., *Macromolecules*, **29** (1996) 7261.
[8] SMITH K. A., VLADKOV M. and BARRAT J.-L., *Macromolecules*, **38** (2005) 571.
[9] AJDARI A. *et al.*, *Physica A*, **204** (1994) 17.
[10] BROCHARD F. and DEGENNES P. G., *Langmuir*, **8** (1992) 3033.
[11] BARRAT J. L. and BOCQUET L., *Phys. Rev. Lett.*, **82** (1999) 4671.
[12] THOMPSON P. A. and TROIAN S. M., *Nature*, **389** (1997) 360.
[13] COTTIN-BIZONNE C. *et al.*, *Nature Mater.*, **2** (2003) 237.
[14] BROCHARD-WYART F. *et al.*, *Langmuir*, **10** (1994) 1566.
[15] ABRAMS C. F. and KREMER K., *Macromolecules*, **36** (2003) 260.
[16] DELLE SITE L., ABRAMS C. F., ALAVI A. and KREMER K., *Phys. Rev. Lett.*, **89** (2002) 156103.
[17] ABRAMS C. F., DELLE SITE L. and KREMER K., *Phys. Rev. E*, **67** (2003) 021807.
[18] DELLE SITE L., LEON S. and KREMER K., *J. Am. Chem. Soc.*, **126** (2004) 2944.
[19] TSCHÖP W., KREMER K. *et al.*, *Acta Polym.*, **49** (1998) 61.
[20] DELLE SITE L., ALAVI A. and ABRAMS C. F., *Phys. Rev. B*, **67** (2003) 193406.
[21] LEON S., DELLE SITE L. and KREMER K., in preparation (2005).
[22] CIEPLAK M., SMITH E. D. and ROBBINS M. O., *Science*, **265** (1994) 1209.
[23] ANDRIENKO D., LEON S., DELLE SITE L. and KREMER K., in preparation (2005).